Supporting information

Stabilized $Cu^{\delta+}$-OH species on Cu nanoparticles encapsulated in porous carbon nitride for electrocatalytic reduction of CO_2 to ethylene

Ling-Wang[a,c,] †, Ji-Long Chen[a,b,] †, Jin Wang[a,b], Yu-Liang Dong[a,b], Wan-Feng Xiong[b], Ze Li[b,d], Duan-Hui Si[b,d] *, Hong-Fang Li[b,d*]， Rong Cao[abd]

[a]College of Chemistry and Chemical Engineering, Xiamen University, Xiamen, 361005, China
[b]State Key Laboratory Structural Chemistry, Fujian Institute of Research on the Structure of Matter Chinese Academy of Sciences, Fuzhou 350002, China
[c]School of new materials, biological and chemical engineering, Jimei Polytechnic Vocational College, Xiamen, 361022 ,China
[d]College of Chemistry and Materials Science, Fujian Normal University, Fuzhou, 350007 ,China

† L.W. and J. C contributed equally
*Corresponding author. E-mail: hongfangli@fjirsm.ac.cn (H-F Li)

Experimental section

Synthesis of Silica Sphere (SiO_2-Sp) Template

Silica spheres (~200 nm diameter) were synthesized via the modified Stöber method. Briefly, 140 mL of anhydrous ethanol, 20 mL of deionized water (DI water), and 4.5 mL of ammonium hydroxide (NH_4OH, 28–30 wt%) were mixed in a flask and stirred at 1000 rpm for 5 min to ensure homogeneity. Subsequently, 5.6 mL of tetraethyl orthosilicate (TEOS) was introduced. The reaction proceeded at room temperature for 1 h under continuous stirring. The resulting silica spheres were collected by centrifugation, washed three times with ethanol, and dried at 60°C.

Synthesis of Porous Graphitic Carbon Nitride (g-C_3N_4)

Porous g-C_3N_4 (denoted as 200-C_3N_4) was synthesized using 200 nm silica spheres as hard templates. First, 2.5 g of melamine and 1.0 g of silica spheres were thoroughly ground. The mixture was then dispersed in 10 mL of anhydrous ethanol via ultrasonication. After ethanol removal by rotary evaporation, the solid was reground and transferred to a covered alumina crucible. Thermal polymerization was conducted in a muffle furnace under static air: the sample was heated from 30°C to 550°C at 5°C

min^{-1} and maintained at 550°C for 5 h. After cooling to room temperature, the yellow product was ground. To remove the silica template, the powder was etched with 20 mL DI water and 5 mL hydrofluoric acid (HF, 40 wt%) at 500 rpm for 24 h. The resulting material was collected by centrifugation, washed with DI water until neutral pH, and dried at 60°C to yield porous 200-C_3N_4.

Synthesis of Cu/200-C_3N_4 Catalysts

The Cu/200-C_3N_4 catalyst was prepared via in situ reduction. Typically, 0.32 g copper(II) sulfate pentahydrate ($CuSO_4 \cdot 5H_2O$), 1.0 g polyvinylpyrrolidone (PVP, MW ≈ 40,000), and 12.8 mg 200-C_3N_4 were dispersed in 100 mL DI water by ultrasonication for 1 h. The homogeneous suspension was transferred to a heated stirrer and maintained at 55°C under stirring. Next, 10 mL of 2 M sodium hydroxide (NaOH) solution was added dropwise, followed by stirring at 55°C for 30 min. Subsequently, 20 mL of 1 M ascorbic acid solution was added under N_2 atmosphere with continued stirring (55°C, 1 h). Finally, an additional 20 mL of 1 M ascorbic acid was introduced, and the temperature was raised to 80°C for 1 h to ensure complete reduction. The resulting precipitate was collected by centrifugation, washed repeatedly with DI water and ethanol, and dried under N_2 atmosphere.

Synthesis of 400-SiO_2-Sp and 600-SiO_2-Sp Template

Synthesis of 400-SiO_2-Sp

Silica spheres with an average diameter of ~400 nm were synthesized via the Stöber method. Two precursor solutions were prepared: Solution A containing 24.75 mL deionized water, 9 mL ammonium hydroxide (28-30 wt%), and 16.25 mL anhydrous ethanol; and Solution B consisting of 4.5 mL tetraethyl orthosilicate (TEOS) in 45.5 mL anhydrous ethanol. Solution A was homogenized by stirring at 1100 rpm for 5 minutes, followed by rapid addition of Solution B. After 1 minute, the stirring rate was reduced to 400 rpm, and the reaction proceeded at room temperature for 2 hours. The resulting silica spheres were collected by centrifugation, washed three times with ethanol, and oven-dried prior to grinding.[1]

Synthesis of 600-SiO_2-Sp

Larger silica spheres (~600 nm) were obtained through seeded growth methodology. First, ~400 nm silica spheres were synthesized following the aforementioned protocol. One-quarter of the as-synthesized colloidal suspension from this initial synthesis was reserved as seed particles. The seeded growth step then replicated the ~400 nm synthesis procedure, with the modification that the reserved seed suspension was incorporated into Solution A before adding Solution B. Subsequent processing - including reaction, centrifugation, washing, and drying - mirrored the standard protocol, yielding monodisperse silica spheres with the target diameter.

Synthesis of 400-C_3N_4 and 600-C_3N_4

400-C_3N_4 and 600-C_3N_4 was synthesized using 400-SiO_2-Sp and 600-SiO_2-Sp as hard templates respectively. First, 2.5 g of melamine and 1.0 g of silica spheres were thoroughly ground. The mixture was then dispersed in 10 mL of anhydrous ethanol via ultrasonication. After ethanol removal by rotary evaporation, the solid was reground and transferred to a covered alumina crucible. Thermal polymerization was conducted in a muffle furnace under static air: the sample was heated from 30°C to 550°C at 5°C min^{-1} and maintained at 550°C for 5 h. After cooling to room temperature, the yellow product was ground. To remove the silica template, the powder was etched with 20 mL DI water and 5 mL hydrofluoric acid (HF, 40 wt%) at 500 rpm for 24 h. The resulting material was collected by centrifugation, washed with DI water until neutral pH, and dried at 60°C to yield porous 400-C_3N_4 and 600-C_3N_4 respectively.

Synthesis of Cu/400-C_3N_4 and Cu/600-C_3N_4Catalysts

Synthesis of Cu/400-C_3N_4

The Cu/200-C_3N_4 catalyst was prepared via in situ reduction. Typically, 0.32 g copper(II) sulfate pentahydrate ($CuSO_4 \cdot 5H_2O$), 1.0 g polyvinylpyrrolidone (PVP, MW ≈ 40,000), and 12.8 mg 400-C_3N_4 were dispersed in 100 mL DI water by ultrasonication for 1 h. The homogeneous suspension was transferred to a heated stirrer and maintained at 55°C under stirring. Next, 10 mL of 2 M sodium hydroxide (NaOH) solution was added dropwise, followed by stirring at 55°C for 30 min. Subsequently, 20 mL of 1 M

ascorbic acid solution was added under N_2 atmosphere with continued stirring (55°C, 1 h). Finally, an additional 20 mL of 1 M ascorbic acid was introduced, and the temperature was raised to 80°C for 1 h to ensure complete reduction. The resulting precipitate was collected by centrifugation, washed repeatedly with DI water and ethanol, and dried under N_2 atmosphere.

Synthesis of Cu/600-C_3N_4

The Cu/200-C_3N_4 catalyst was prepared via in situ reduction. Typically, 0.32 g copper(II) sulfate pentahydrate ($CuSO_4 \cdot 5H_2O$), 1.0 g polyvinylpyrrolidone (PVP, MW ≈ 40,000), and 12.8 mg 600-C_3N_4 were dispersed in 100 mL DI water by ultrasonication for 1 h. The homogeneous suspension was transferred to a heated stirrer and maintained at 55°C under stirring. Next, 10 mL of 2 M sodium hydroxide (NaOH) solution was added dropwise, followed by stirring at 55°C for 30 min. Subsequently, 20 mL of 1 M ascorbic acid solution was added under N_2 atmosphere with continued stirring (55°C, 1 h). Finally, an additional 20 mL of 1 M ascorbic acid was introduced, and the temperature was raised to 80°C for 1 h to ensure complete reduction. The resulting precipitate was collected by centrifugation, washed repeatedly with DI water and ethanol, and dried under N_2 atmosphere.

Synthesis of Cu NPs

The Cu/200-C_3N_4 catalyst was prepared via in situ reduction. Typically, 0.32 g copper(II) sulfate pentahydrate ($CuSO_4 \cdot 5H_2O$) and 1.0 g polyvinylpyrrolidone (PVP, MW ≈ 40,000) were dispersed in 100 mL DI water by ultrasonication for 1 h. The homogeneous suspension was transferred to a heated stirrer and maintained at 55°C under stirring. Next, 10 mL of 2 M sodium hydroxide (NaOH) solution was added dropwise, followed by stirring at 55°C for 30 min. Subsequently, 20 mL of 1 M ascorbic acid solution was added under N_2 atmosphere with continued stirring (55°C, 1 h). Finally, an additional 20 mL of 1 M ascorbic acid was introduced, and the temperature was raised to 80°C for 1 h to ensure complete reduction. The resulting precipitate was collected by centrifugation, washed repeatedly with DI water and ethanol, and dried under N_2 atmosphere.

Electrochemical Measurements

Electrocatalytic CO_2 reduction reaction (CO_2RR) performance was evaluated in a custom-made gas diffusion electrode (GDE) flow cell (model: 101016, Tianjin Gaoss Union Technology Co., Ltd.) at ambient temperature and pressure, using a CHI1140c electrochemical workstation (Shanghai CH Instrument Co., Ltd.). The electrolyte was 1 M potassium hydroxide (KOH) solution. The working electrode was prepared by drop-casting catalyst ink onto a carbon paper gas diffusion layer (GDL, Toray YLS-30T). The carbon paper was cut to dimensions of 1 cm × 3 cm, and 80 μL of catalyst ink (loading: 0.4 mg cm^{-2}) was uniformly deposited onto a defined 1 cm^2 active area. The catalyst ink was prepared by dispersing 5 mg of catalyst in a mixture of 960 μL of isopropanol and 40 μL of Nafion solution (5 wt%, Adamas) followed by ultrasonication for 30 minutes. A platinum foil served as the counter electrode, and an Ag/AgCl electrode (saturated KCl) was used as the reference electrode. An anion exchange membrane (FAA-PK-130, FuMA-Tech GmbH) separated the cathodic and anodic compartments. During testing, CO_2 gas was fed to the cathode chamber at a flow rate of 20 mL min^{-1}, and the electrolyte was circulated at 20 mL min^{-1}. Prior to CO_2RR measurements, the catalyst was activated by performing cyclic voltammetry (CV) scans from 0 V to -1.0 V vs. RHE at a scan rate of 100 mV s^{-1} for 10 cycles to stabilize the catalyst surface.

During the test, the flow rate of CO_2 was maintained at 20 sccm and the flow rate of electrolyte was maintained at 20 ml min^{-1}. All potentials were referenced to reversible hydrogen electrode (RHE) with the formula of $E_{vs.\ RHE} = E_{vs.\ Ag/AgCl} + 0.197 + 0.0592\ pH$. LSV curves were collected with the scan rate of 10 mV/s from 0 to -1.2 V *vs.* RHE. The CO_2 electroreduction at different current densities measured by chronopotentiometry. Gas products were detected by gas chromatography fitted with a thermal conductivity detector and a flame ionization detector (GC-9790plus, Fuli). The liquid solution with DMSO standard was then quantitatively analyzed by NMR (JES-ECZ600S, JEOL).

The gas product Faradic efficiency was calculated by the following equation:

$$FE_{gas} = \frac{p \times v \times f \times 10^{-6}(m^3/ml)}{RT} \times \frac{n_e F}{I \times 60(s/min)} \times 100\%$$

Where p is the pressure (1.013×10^5 Pa); v is the volumetric concentration of gas product determined from GC (in ppm); f is the gas flow rate (20 ml min^{-1}); n_e is the number of electrons required to generate the product; F is the Faradaic constant (96485 C mol^{-1}); R is the ideal gas constant (8.314 J mol^{-1} K^{-1}); T is the room temperature (298 K); I is the total current.

The Faradaic efficiency of liquid product is:

$$FE_{liquid} = \frac{\text{moles of product}}{Q / nF} \times 100\%$$

Where Q is the total charge in a period of reaction time (C); n is the number of electrons required to generate the product; F is the Faradaic constant (96485 C mol^{-1}).

Characterization measurement

Electrochemical Active Surface Area (ECSA) Measurement

The electrochemical active surface area (ECSA) of Cu catalysts was determined via lead underpotential deposition (Pb UPD). Measurements were performed in a single-compartment electrochemical cell using a catalyst-modified glassy carbon electrode (GCE) as the working electrode, an Ag/AgCl reference electrode, and a carbon rod counter electrode. The electrolyte consisted of 0.1 M $HClO_4$ containing 0.5 mM $PbCl_2$ and 50 mM KCl. Prior to testing, dissolved oxygen was removed by purging the electrolyte with high-purity N_2(g) for 30 min. A constant deposition potential of -0.375 V vs. Ag/AgCl was applied for 10 min. Linear sweep voltammetry (LSV) was then performed from -0.5 V to -0.1 V vs. Ag/AgCl at a scan rate of 0.01 V s^{-1}. The charge density associated with the oxidative stripping of the deposited Pb monolayer was obtained by integrating the area under the Pb stripping peak. ECSA was calculated assuming complete monolayer coverage and a 2-electron transfer process per Pb atom, corresponding to a charge density of 310 μC cm^{-2} for a smooth polycrystalline Cu surface. The ECSA was calculated using the formula:

$$ECSA\_absolute = \frac{s/v}{310 \times 10^{-6}}\ cm^2$$

where Q is the integrated charge (in coulombs, C) from the stripping peak.

To enable a comparison of the intrinsic active site density, the ECSA was normalized by the mass of the catalyst loaded on the working electrode (m, in mg):

$$\text{ECSA} = \frac{ECSA\_absolute}{m} \ \text{cm}^2\,\text{mg}^{-1}$$

In Situ Attenuated Total Reflection Infrared Spectroscopy (ATR-IR)

In situ ATR-IR spectroscopy was employed to identify adsorbed reaction intermediates during the CO_2 reduction reaction (CO_2RR). Experiments utilized an in situ electrochemical cell (Beijing Zhongyan Huanke Technology Co., Ltd.) coupled to a Nicolet 700 FTIR spectrometer (Thermo Fisher Scientific) equipped with a liquid-nitrogen-cooled mercury cadmium telluride (MCT) detector. A catalyst ink was drop-cast onto a glassy carbon working electrode, paired with a Pt wire counter electrode and an Ag/AgCl reference electrode. The electrolyte (0.1 M KCl + 0.1 M $KHCO_3$) was saturated with CO_2(g) by purging for 30 min prior to measurements. Spectra were acquired at various applied potentials, with each spectrum representing an average of 32 scans at 4 cm^{-1} resolution.

In Situ Raman Spectroscopy

In situ Raman spectroscopy was performed to monitor structural changes of reaction intermediates and catalyst interactions under CO_2RR conditions. Measurements were conducted using a Labram HR confocal Raman microscope (Shimadzu) integrated with a C031-4 in situ electrochemical cell (Gaoss Union). The working electrode (catalyst-coated glassy carbon), Ag/AgCl reference electrode, and Pt wire counter electrode were identical to those used for ATR-IR. The electrolyte (0.1 M KCl + 0.1 M $KHCO_3$) was CO_2-saturated by purging for 30 min. Spectra were collected at different applied potentials using a 633 nm laser excitation source.

Density Functional Theory (DFT) Calculations

Density functional theory (DFT) calculations were performed using the Vienna Ab initio Simulation Package (VASP) to elucidate the CO_2RR mechanism at the Cu/200-

C_3N_4 interface.[1-4] Reaction pathways were modeled on both Cu/200-C_3N_4 (represented as melamine-covered Cu(111)) and Cu nanoparticles (modeled via the Cu(111) facet). The projector augmented wave (PAW)[5, 6] method was employed with the Perdew-Burke-Ernzerhof (PBE) generalized gradient approximation (GGA) functional[7], incorporating Grimme's DFT-D3 correction[8] for van der Waals interactions. A plane-wave cutoff energy of 400 eV was used. The Brillouin zone was sampled using (3×3×1) Monkhorst-Pack k-point grids.

Surface models consisted of a five-layer slab with a (5×5) surface unit cell and a 15 Å vacuum layer. The top four atomic layers and adsorbates were fully relaxed, while the bottom layer remained fixed. Structural optimizations were considered converged when energy differences between successive steps were $< 1\times10^{-4}$ eV and forces on all relaxed atoms were < 0.05 eV $Å^{-1}$.

Gibbs free energies (ΔG) for reaction intermediates were calculated using the computational hydrogen electrode (CHE) model[9] at 298.15 K:

$$\Delta G_0 = \Delta E_{DFT} + \Delta E_{ZPE} - T\Delta S$$

where E_{DFT} is the electronic energy difference, E_{ZPE} is the difference in zero-point energy, and ΔS is the entropy difference. The ΔG_0 values were computed using the VASPKIT package[10]. The optimized atomic structure of the Cu/200-C_3N_4 model is depicted in Fig.S15

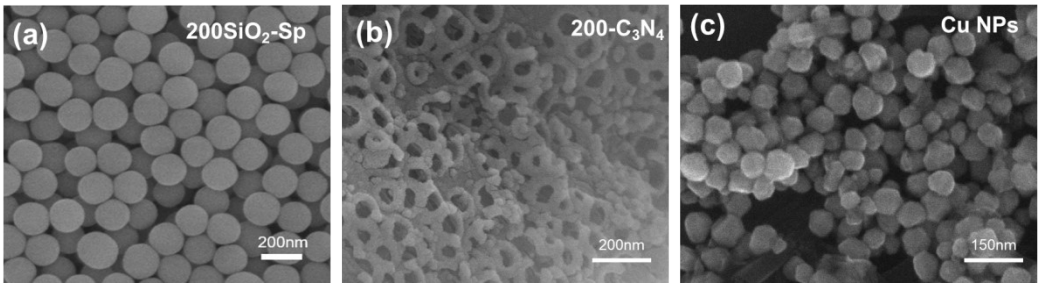

Fig. S1. SEM images of (a) 200 SiO_2-Sp (b) 200-C_3N_4 and (c) Cu NPs.

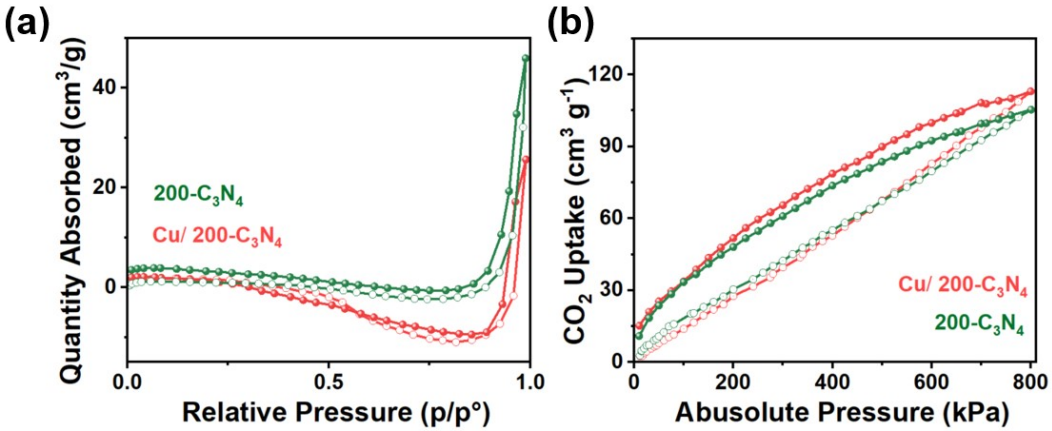

Fig. S2. (a) Nitrogen adsorption-desorption isotherm (b) CO_2 adsorption isotherm. For 200-C_3N_4 and Cu/200-C_3N_4

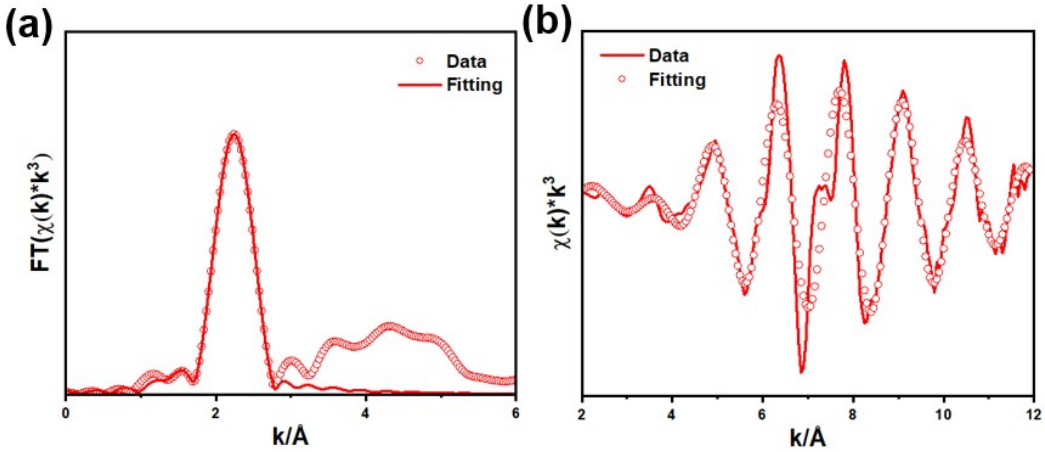

Fig. S3. Cu K-edge EXAFS and curvefit for Cu/200-C_3N_4 shown in (a) k^3-weighted k-space (b) k^3-weighted R-space.

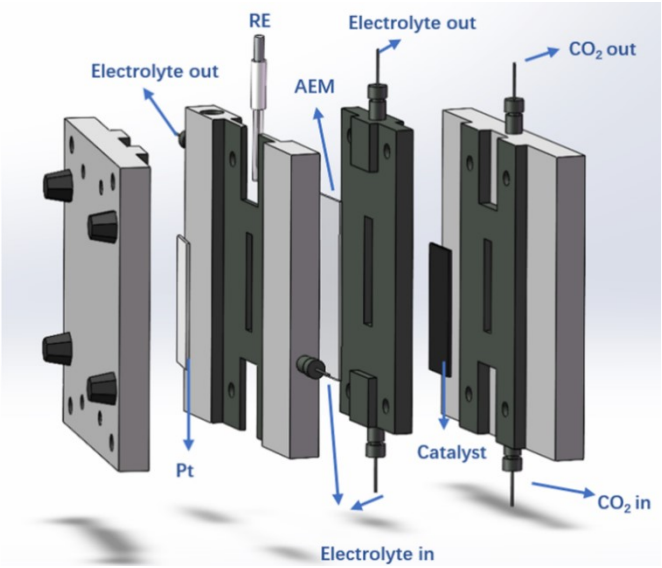

Fig. S4. Schematic diagram of the flow cell used for eCO_2RR experiments.

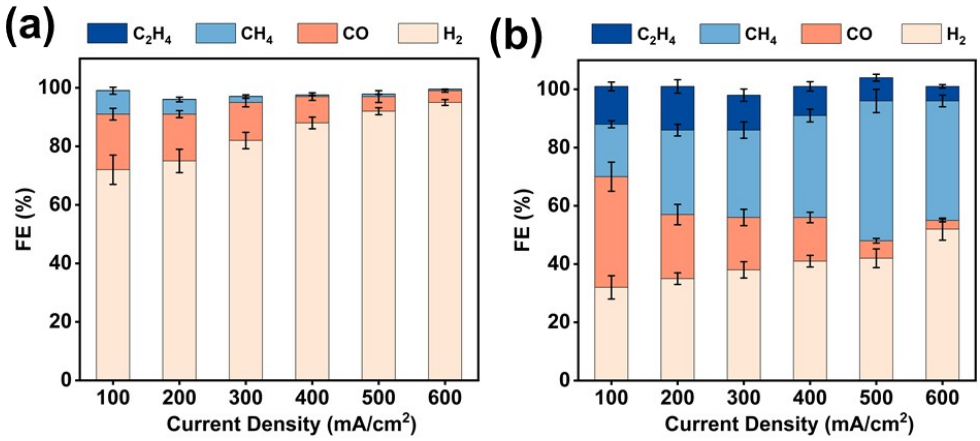

Fig. S5. The Faradaic efficiency of (a) 200-C_3N_4 and (b) Cu NPs at different current densities.

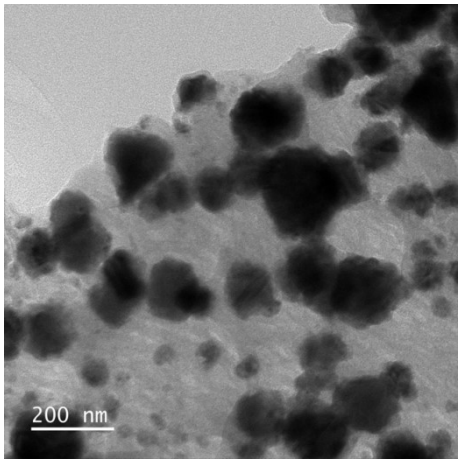

Fig. S6. TEM images of Cu/200-C_3N_4 after CO_2RR durability test.

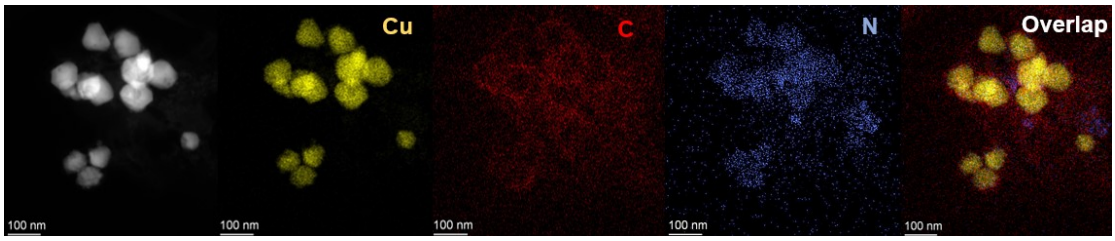

Fig. S7. STEM-mapping images of Cu/200-C_3N_4 after CO_2RR durability test.

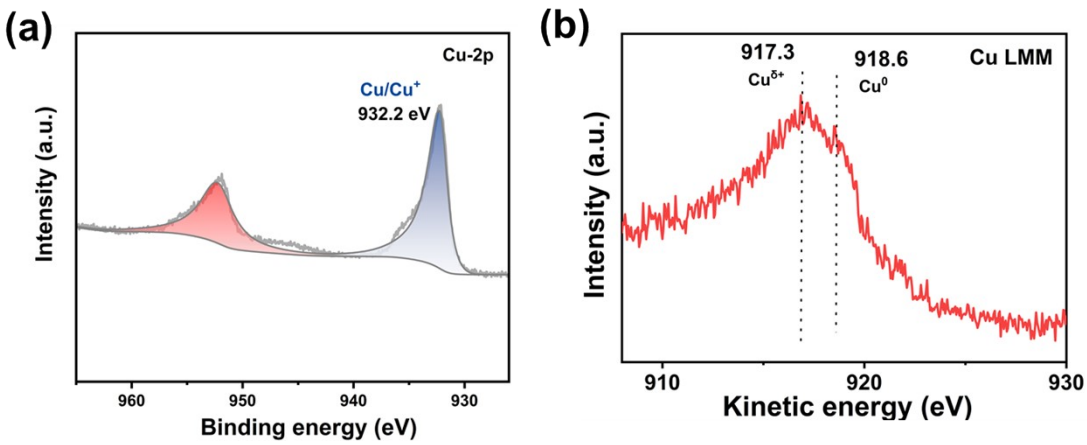

Fig. S8. The XPS of (a) Cu 2p (b) Cu LMM for Cu/200-C_3N_4 after CO_2RR durability test.

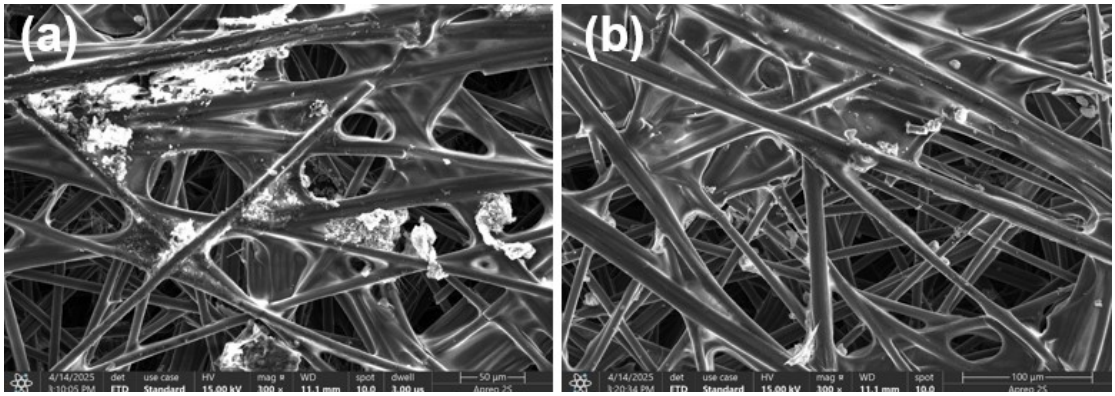

Fig. S9. TEM images of carbon paper after CO_2RR durability test for (a) Cu NPs and (b) Cu/200-C_3N_4.

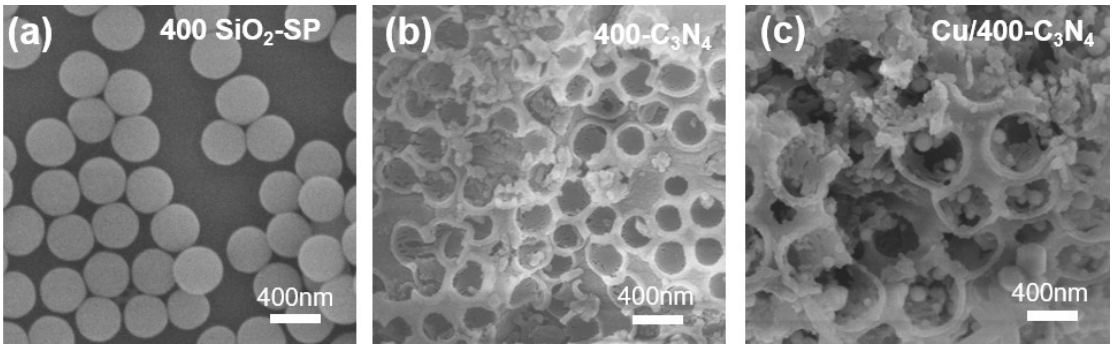

Fig. S10. SEM images of (a) 400 SiO_2-SP (b) 400-C_3N_4 and (c) Cu/400-C_3N_4.

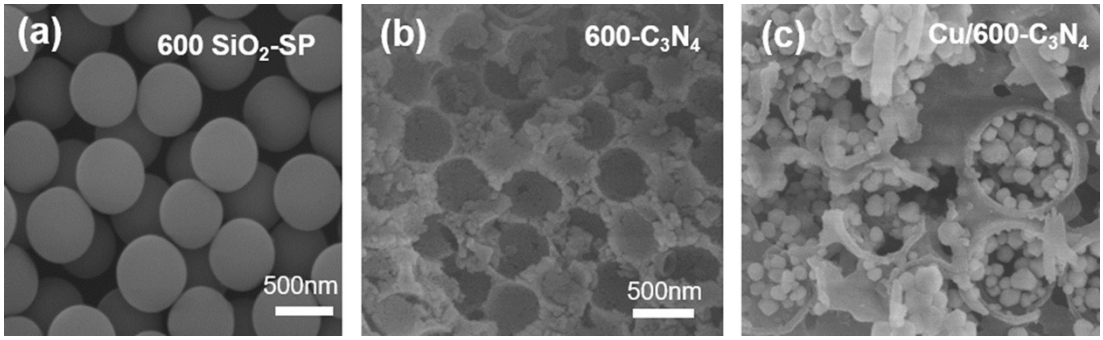

Fig. S11. SEM images of (a) 600 SiO_2-SP (b) 600-C_3N_4 and (c) Cu/600-C_3N_4.

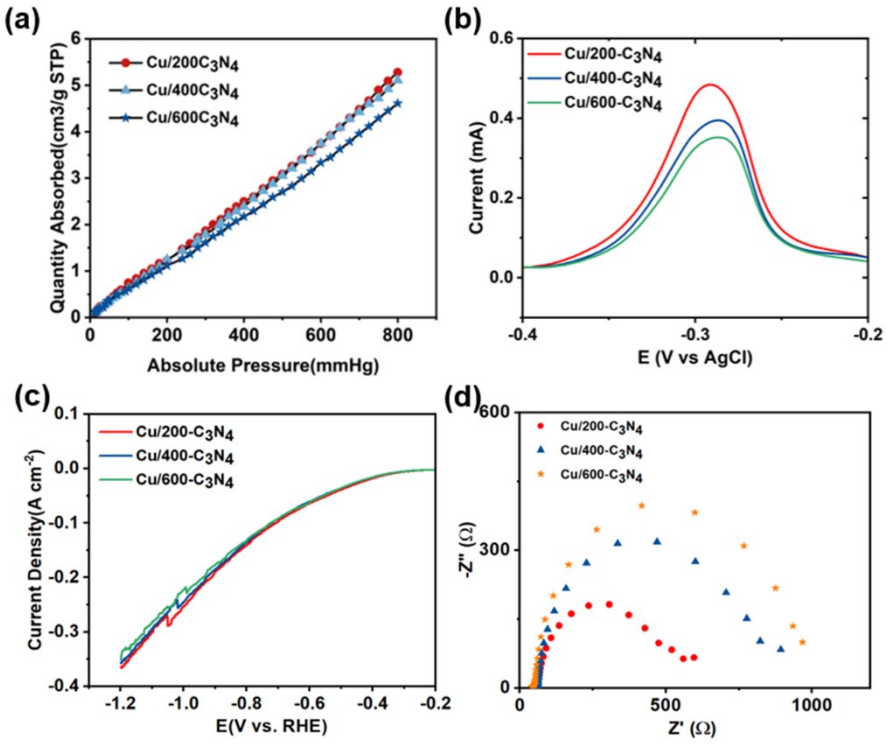

Fig. S12. (a) CO_2 adsorption curves of catalysts Cu/200-C_3N_4, Cu/400-C_3N_4 and Cu/600-C_3N_4;(b) The LSV curves of underpotential deposited Cu/200-C_3N_4, Cu/400-C_3N_4 and Cu/600-C_3N_4; (c) The LSV curves of Cu/200-C_3N_4 Cu/400-C_3N_4 and Cu/600-C_3N_4 in 1 M KOH solution under CO_2 atmosphere; (d) EIS curve of Cu/200-C_3N_4 Cu/400-C_3N_4 and Cu/600-C_3N_4.

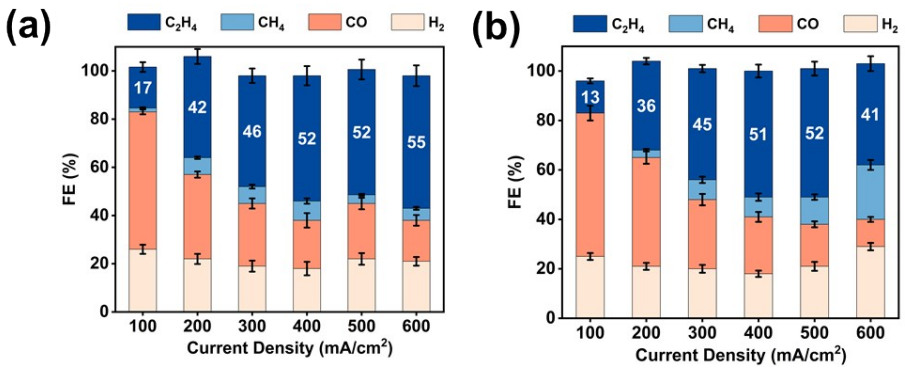

Fig. S13. The Faradaic efficiency of (a) Cu/400-C_3N_4 and (b) Cu/600-C_3N_4 at different current densities.

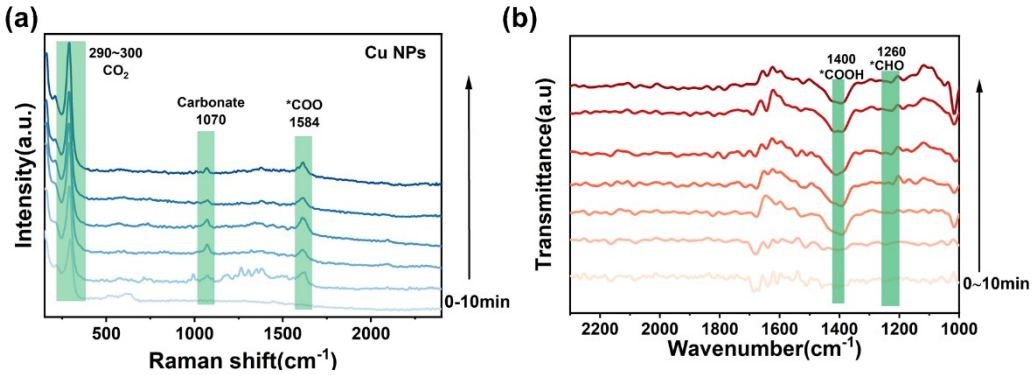

Fig. S14. (a) In-situ Raman spectra of Cu NPs recorded at –1.1 V vs. RHE over 10 min; (b) In-situ ATR-FTIR spectra of Cu NPs recorded at –1.1 V vs. RHE over 10 min.

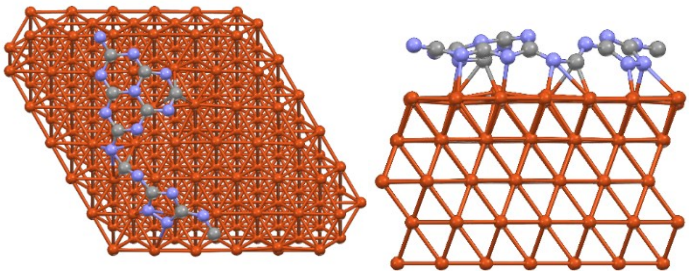

Fig. S15. The structural models of Cu/200-C_3N_4.

Table S1. Curvefit parameters for Cu K-edge EXAFS for Cu-based nanoreactors

sample	path	$\triangle E_0$	N	R / Å	δ^2 / Å^2	R factor
Cu/200-C_3N_4	Cu-Cu	4.36	9.14	2.5459	0.00871	0.0059
	Cu-N		0.49	1.8407	0.00024	

So^2 was fixed as 0.818 (by Cu foil).

Table S2. Comparison of CO_2RR performance in reported Cu-based catalysts

Catalyst	Cell type	Electrolyte	E (V *vs.* RHE)	C_2H_4 FE (%)	J_{total} (mA/cm^2)	Ref.
Cu/200-C3N4	Flow cell	1 M KOH	-1.8	57	600	This work
CuODA	H-cell	1 M KOH	-0.9	55.5	300	Ref. 11
Phase-sepa-rated CuPd	Flow cell	1 M KOH	-0.7	47	360	Ref. 12
Cu-MOF	H-cell	0.1 M $KHCO_3$	-1.0	50	7	Ref. 13
ZnCu-NSAs	H-cell	0.5 M $KHCO_3$	-0.8	60	92	Ref. 14
CuO-SH	Flow cell	0.1 M $KHCO_3$	-1.2	79.5	304	Ref. 15
PcCu-Cu-O	H-cell	0.1 M $KHCO_3$	-1.2	50	7	Ref. 16

Reference

1. X. Hai, Y. Zheng, Q. Yu, N. Guo, S. Xi, X. Zhao, S. Mitchell, X. Luo, V. Tulus, M. Wang, X. Sheng, L. Ren, X. Long, J. Li, P. He, H. Lin, Y. Cui, X. Peng, J. Shi, J. Wu, C. Zhang, R. Zou, G. Guillén-Gosálbez, J. Pérez-Ramírez, M. Koh, Y. Zhu, J. Li and J. Lu, Geminal-atom catalysis for cross-coupling, *Nature*, 2023, DOI: 10.1038/s41586-023-06529-z, 19.
2. G. Kresse and J. Hafner, Ab initio molecular-dynamic simulation of the Liquid-Metal Amorphours-Semiconductor transition in germanium, *Phys. Rev. B*, 1994, **49**, 14251–14269.
3. G. Kresse and J. Furthmuller, Efficiency of ab-initio total energy calculations for metals and semiconductors using a plane-wave basis set, *Comput. Mater. Sci.*, 1996, **6**, 15–50.
4. G. Kresse and J. Furthmuller, Efficient iterative schemes for ab initio total-energy calculations using a plane-wave basis set, *Phys. Rev. B*, 1996, **54**, 11169–11186.
5. P. Blochl, Projector Augmented-Wave method, *Phys. Rev. B*, 1994, **50**, 17953–17979.
6. G. Kresse and D. Joubert, From ultrasoft pseudopotentials to the projector augmented-wave method, *Phys. Rev. B*, 1999, **59**, 1758–1775.

7. J. Perdew, K. Burke and M. Ernzerhof, Generalized gradient approximation made simple, *Phys. Rev. Lett.*, 1996, **77**, 3865–3868.
8. S. Grimme, Density functional theory with London dispersion corrections, *Wiley Interdiscip. Rev.-Comput. Mol. Sci.*, 2011, **1**, 211–228.
9. J. Norskov, J. Rossmeisl, A. Logadottir, L. Lindqvist, J. Kitchin, T. Bligaard and H. Jónsson, Origin of the overpotential for oxygen reduction at a fuel-cell cathode, *J. Phys. Chem. B*, 2004, **108**, 17886–17892.
10. V. Wang, N. Xu, J. Liu, G. Tang and W. Geng, VASPKIT: A user-friendly interface facilitating high-throughput computing and analysis using VASP code, *Comput. Phys. Commun.*, 2021, **267**, 19.
11. J. Hu, S. Osella, J. Albero and H. García, Unraveling the Influence of Shell Thickness in Organic Functionalized Cu_2O Nanoparticles on C_{2+} Products Distribution in Electrocatalytic CO_2 Reduction, *Adv. Funct. Mater.*, 2024, **34**, 11.
12. M. Li, Y. Ma, J. Chen, R. Lawrence, W. Luo, M. Sacchi, W. Jiang and J. Yang, Residual Chlorine Induced Cationic Active Species on a Porous Copper Electrocatalyst for Highly Stable Electrochemical CO_2 Reduction to C_{2+}, *Angew. Chem.-Int. Edit*., 2021, **60**, 11487–11493.
13. L. Wang, X. Li, L. Hao, S. Hong, A. Robertson and Z. Sun, Integration of ultrafine CuO nanoparticles with two-dimensional MOFs for enhanced electrochemical CO_2 reduction to ethylene, *Chin. J. Catal.*, 2022, **43**, 1049–1057.
14. X. Zhang, B. Ren, H. Li, S. Liu, H. Xiong, S. Dong, Y. Li, D. Luo, Y. Cui, G. Wen and X. Wang, Regulating ethane and ethylene synthesis by proton corridor microenvironment for CO_2 electrolysis, *J. Energy Chem*., 2023, **87**, 368–377.
15. Y. Yao, T. Shi, W. Chen, J. Wu, Y. Fan, Y. Liu, L. Cao and Z. Chen, A surface strategy boosting the ethylene selectivity for CO_2 reduction and in situ mechanistic insights, *Nat. Commun.*, 2024, **15**, 10.
16. X. Qiu, H. Zhu, J. Huang, P. Liao and X. Chen, Highly Selective CO_2 Electroreduction to C_2H_4 Using a Metal-Organic Framework with Dual Active Sites, *J.Am.Chem.Soc*, 2021, **143**, 7242–7246.